Electrical and Computer Engineering Faculty Research & Creative Works

Electrical and Computer Engineering

A Novel Microwave Method for Detection of Long Surface Cracks in Metals

Chin-Yung Yeh

R. Zoughi
Missouri University of Science and Technology, zoughi@mst.edu

Recommended Citation

C. Yeh and R. Zoughi, "A Novel Microwave Method for Detection of Long Surface Cracks in Metals," *IEEE Transactions on Instrumentation and Measurement*, vol. 43, no. 5, pp. 719-725, Institute of Electrical and Electronics Engineers (IEEE), Oct 1994.
The definitive version is available at https://doi.org/10.1109/19.328896

A Novel Microwave Method for Detection of Long Surface Cracks in Metals

Chin-Yung Yeh and Reza Zoughi, *Senior Member, IEEE*

Abstract— A novel microwave technique for detecting long surface cracks in metals is described. This technique utilizes an open-ended waveguide to probe the surface of a metal. In the absence of a crack the metal surface is seen as a relatively good short-circuit load. However, in the presence of a crack higher order modes are generated which in turn change the reflection properties at the waveguide aperture. This change brings about a perturbation in the standing wave characteristics which is then probed by a diode detector. The experimental and theoretical foundations of this technique are given, along with several examples. It is shown that cracks a fraction of a millimeter in width are easily detected at around 20 GHz or lower. Smaller cracks can be detected at higher microwave frequencies.

I. INTRODUCTION

METAL FATIGUE or failure usually begins from the surface. Aircraft fuselage, nuclear power plant steam generator tubing, and steel bridges are examples of environments in which this type of metal failure occurs. Hence, fatigue and stress crack detection on metallic structures is of utmost importance to the on-line and in-service inspections of metallic components. Currently there are several prominent nondestructive testing (NDT) techniques for detecting surface cracks in metals; however, each method possesses certain limitations and disadvantages. In some environments the technique used may not be an optimum one, but the only one that can be applied. Acoustic emission testing, dye penetrant testing, eddy current testing, ultrasonic testing, radiographic testing, and magnetic particle testing are examples of these techniques [1].

Since the late sixties there have been several researchers who have attempted using microwaves for surface crack detection on metals, with modest success. Microwave techniques offer certain advantages, when detecting hairline stress or fatigue cracks, such as: the sensor may or may not be in contact with the surface under examination; they are applicable in high-temperature environments; the crack may be filled with dielectric materials such as dirt, paint or rust, or the surface of the metal may be covered with paint or a similar compound and the crack may still be detected. Finally polarization properties of microwaves can provide information regarding relative crack orientation. Microwaves have also shown the potential of estimating crack width, depth and length. Feinstein *et al.* [2]–[4] used a mode conversion technique based on the

idea that the crack converts a portion of the incident wave to an orthogonally polarized wave. This noncontact technique utilizes a microwave bridge for nulling out background signals, and a microwave rotary joint for producing incident waves of different polarizations. They were able to detect cracks with widths of 0.05 mm and different depths. The drawbacks of this technique are the introduction of the additional loss associated with the microwave bridge and the low-frequency mechanical modulation associated with the rotary joint. Bahr [5] used a similar technique at 100 GHz. He used mode conversion without polarization modulation. To separate the orthogonally polarized wave from the copolarized backscattered wave an orthomode coupler was utilized. To increase the spatial resolution of the measurement apparatus, he used a focusing lens on a horn antenna to create a beamwidth equivalent to 3.5 mm at the focal point. The integrity of this approach was checked by examining 0.25 mm wide cracks on aluminum plates. He showed that at high enough frequencies, the depth of a crack may also be determined. The disadvantage of this method is that detection is directly dependent on the degree of decoupling between the orthogonally polarized signals created by the mode conversion in the crack. He also used circularly polarized signals and a dielectric waveguide to improve detection sensitivity such that fatigue cracks under loading were detected [6]. Other microwave approaches have included microstrip planar lines and ferromagnetic resonance probes for crack detection [7]–[14].

This paper describes a new and simpler microwave technique for detecting long and straight surface cracks using an open-ended waveguide. The experimental and theoretical foundations of this technique along with several results are described.

II. APPROACH

A. Experimental Foundation

In mid-1992 several experiments, using an open-ended waveguide, were conducted to investigate the feasibility of using this probe to detect long surface cracks in metals. In this context, long refers to a crack whose length is greater than or equal to the broad dimension of a waveguide. Various long cracks of different widths and depths were milled on top of flat metal sheets. Preliminary experiments were conducted by moving (using a computer-controlled stepping motor) the cracked metal surface over the aperture of the open-ended waveguide while monitoring the standing-wave characteristics inside the waveguide. Subsequently, it was observed that when
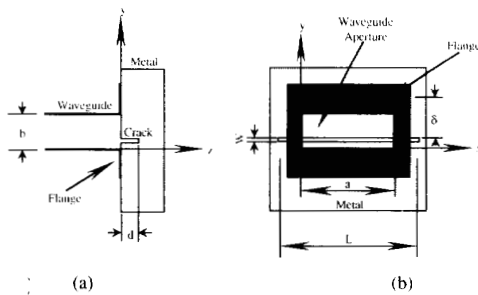
Fig. 1.   Geometry of a surface crack and a waveguide aperture: (a) side view, (b) plane view.

the crack axis (length) is parallel to the broad dimension of the waveguide (orthogonal to the electric field of the dominant TE_{10} mode) the standing wave experiences a pronounced shift in location when the crack is exposed to the aperture of the waveguide compared to when the crack is outside the aperture (a short-circuit condition). This shift indicates changes in the reflection coefficient properties of the metal surface perturbed by the crack. It was also observed that this shift is highly dependent on the relative location of the crack within the waveguide aperture (i.e., whether the crack is at the edge or at the center of the aperture). Fig. 1 shows the geometry of a crack with width W, depth d, and length L and a waveguide aperture with dimensions a and b, when the crack length is parallel to the broad dimension of the waveguide, and δ is a dimension indicating the location of the crack relative to an arbitrary location on the small dimension of the waveguide aperture, b. It was also observed that when the crack was not parallel to the broad dimension of the waveguide, the level of change in the standing wave decreased, and when the crack became parallel to the smaller dimension of the waveguide (parallel to the dominant TE_{10} mode electric field) there was no measurable perturbation in the characteristics of the standing wave. This is due to the fact that in this case the surface currents on the metal surface are parallel to the crack length which does not disturb the surface currents. It must be noted here that most fatigue and stress cracks in real life are not straight. However, they can usually be considered fairly straight along their lengths.

Fig. 2 shows a simple measurement apparatus that was used for these experiments. An oscillator feeds a (slotted) waveguide terminated by a metal plate in which there is a crack. Placing the diode detector a distance l away from the waveguide aperture, the metal plate can be scanned by the waveguide aperture and the standing voltage recorded. As will be seen later, different detector locations, l, will change the difference between the measured signals for the short-circuit case and when the crack is in the middle of the aperture. If l is chosen such that the detector is located between a maximum and a minimum on the standing- wave pattern, this difference is maximized.

At 24 GHz, a long crack with $L > 10.7$ mm, $W = 0.84$ mm, and $d = 1.03$ mm was scanned over the aperture of a K-band waveguide ($a = 10.67$ mm and $b = 4.32$ mm). The diode output voltage measured at $l = 9.45$ cm is shown in Fig. 3 (the solid line). The results indicate that while the crack is outside
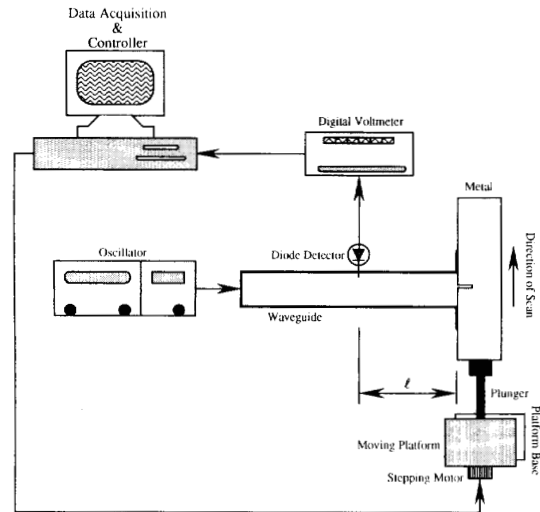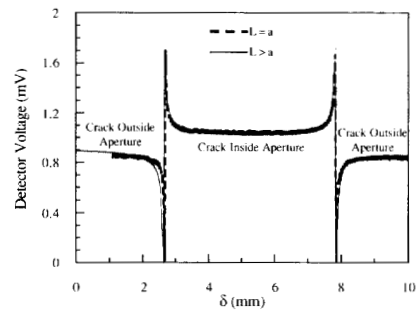

Fig. 2.   Measurement apparatus.

Fig. 3.   Experimental characteristics signal at 24 GHz for a crack with $W = 0.84$ mm and $d = 1.03$ mm: (———) $L > 10.7$ mm, (- - - - -) $L = 10.7$ mm.

the waveguide aperture the diode registers very little voltage variation due to the fact that the waveguide is terminated by a short circuit. The noise-like feature associated with the signal is due to the quantization resolution of the A/D converter and the internal noise of the voltmeter. As the crack begins to appear within the waveguide aperture the voltage experiences a rapid magnitude change which is an indication of rapid phase change in the reflection coefficient at the aperture. The same phenomenon occurs when the crack leaves the waveguide aperture. The voltage value does not change very much while the crack is inside the aperture; however, its value is still different than that of a short-circuit case. The diode output voltage as a function of δ (here on referred to as the *crack characteristics signal*) is clearly an indication of the presence of a crack (*detection*), since the absence of the crack results in a fairly constant voltage.

B. Theoretical Foundation

To theoretically model this phenomenon an effort was made to simplify the geometry of the crack with respect to the waveguide. It was decided to investigate the effect of crack length on the characteristic signals. The idea was that
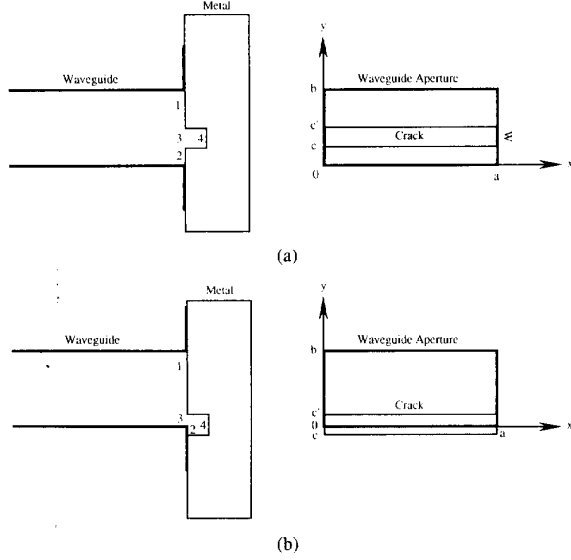
Fig. 4. Relative crack geometry with respect to the waveguide aperture and the coordinate system: (a) crack completely inside the aperture, (b) crack partially inside the aperture.

if the length of the crack is approximated to be equal to the broad dimension of the waveguide aperture, a, then the problem could be modeled as a large waveguide feeding a much narrower short-circuited waveguide with the same broad dimension. Subsequently, an experiment was conducted in which a crack with the same width and depth as those used for the solid line in Fig. 3 but with $L = 10.7$ mm (equal to the broad dimension of the waveguide) was used to determine its characteristic signal at 24 GHz. The dashed line in Fig. 3 shows the results of this experiment. Comparing the solid and the dashed line clearly indicates that, for thin cracks (small W), once the length extends beyond the waveguide aperture there will not be any considerable perturbation in the standing-wave pattern. Thus, in the subsequent theoretical derivations we can assume that the length of a crack is equal to the broad dimension of the waveguide, a. The slight widening of the characteristic signal at around $\delta = 2.5$ mm for the long crack (solid line) is attributed to a small amount of radiation through the long crack. This problem becomes much less important as the width of a crack becomes small which is the case for many fatigue cracks.

Fig. 4 shows the relative geometry of a crack with respect to the waveguide aperture and the coordinate system used for the modeling. The crack dimension is $W \times d \times a$, and W extends from c to c' in the y direction. The dominant mode propagating in the $+z$ direction is incident upon the waveguide aperture. The reflected wave propagates in the $-z$ direction, and a standing wave is formed inside the waveguide. The properties of the standing wave are influenced by the crack size and its location within the waveguide aperture. The reflected wave arises as a direct consequence of forcing the boundary conditions inside and outside the crack at all times. Only those field components used to force the boundary conditions are listed below.

The dominant TE_{10} mode in the waveguide is the incident wave whose electric and magnetic fields are given by [15]

$$E_y^i = \sin \frac{\pi x}{a} e^{-j\beta_1 z} \tag{1}$$

$$H_x^i = \frac{-1}{\eta_1} \sin \frac{\pi x}{a} e^{-j\beta_1 z} \tag{2}$$

where

$$\beta_1 = \sqrt{k_0^2 - \left(\frac{\pi}{a}\right)^2}, \quad k_0 = \frac{2\pi}{\lambda_0}, \quad \eta_1 = \frac{k_0 \eta_0}{\beta_1}, \eta_0 = \sqrt{\frac{\eta_0}{\varepsilon_0}}$$

and where λ_0, k_0, η_0 and μ_0 are the free-space wavelength, wavenumber, permittivity and permeability, respectively. η_0 and η_1 are the free-space and waveguide intrinsic impedances, respectively. In the presence of a crack the electric field bends around the crack, and consequently generates an infinite number of higher order TM modes. Thus, the reflected wave in the waveguide, due to the crack, consists of the reflected TE_{10} mode (since the crack length and waveguide broad dimension are assumed equal) given by

$$E_{y_{TE}}^r = A_{10} \sin \frac{\pi x}{a} e^{j\beta_1 z} \tag{3}$$

$$H_{x_{TE}}^r = \frac{A_{10}}{\eta_1} \sin \frac{\pi x}{a} e^{j\beta_1 z}. \tag{4}$$

The reflected TM modes are given by

$$E_{y_{TM}}^r = \sum_{m=1}^{\infty} A_{1m} \sin \frac{\pi x}{a} \cos \frac{m\pi y}{b} e^{j\beta_{1m}^b z} \tag{5}$$

$$H_{x_{TM}}^r = \sum_{m=1}^{\infty} \frac{A_{1m}}{\eta_{1m}^b} \sin \frac{\pi x}{a} \cos \frac{m\pi y}{b} e^{j\beta_{1m}^b z} \tag{6}$$

where A_{10} and A_{1m} $(m = 1, 2, 3, \ldots)$ are unknown coefficients to be determined and

$$\beta_{1m}^b = \sqrt{k_0^2 - \left(\frac{\pi}{a}\right)^2 - \left(\frac{m\pi}{b}\right)^2}, \quad \eta_{1m}^b = \frac{\beta_{1m}^b \eta_0}{k_0}.$$

The waves in the crack consist of forward and reflected TE_{10} modes given by

$$E_{y_{TE}} = \left(B_{10} e^{-j\beta_1 z} + C_{10} e^{j\beta_1 z}\right) \sin \frac{\pi x}{a} \tag{7}$$

$$H_{x_{TE}} = \frac{1}{\eta_1} \left(-B_{10} e^{-j\beta_1 z} + C_{10} e^{j\beta_1 z}\right) \sin \frac{\pi x}{a} \tag{8}$$

and forward and reflected TM modes given by

$$E_{y_{TM}} = \sum_{m=1}^{\infty} \left(B_{1m} e^{-j\beta_{1m}^c z} + C_{1m} e^{j\beta_{1m}^c z}\right)$$
$$\times \sin \frac{\pi x}{a} \cos \frac{m\pi(y - c)}{W} \tag{9}$$

$$H_{x_{TM}} = \sum_{m=1}^{\infty} \left(-B_{1m} e^{-j\beta_{1m}^c z} + C_{1m} e^{j\beta_{1m}^c z}\right)$$
$$\times \frac{1}{\eta_{1m}^c} \sin \frac{\pi x}{a} \cos \frac{m\pi(y - c)}{W} \tag{10}$$

where B_{10}, C_{10}, B_{1m} and C_{1m} $(m = 1, 2, 3, \ldots)$ are coefficients to be determined. W, which is the crack width, is equal

to $(c' - c)$ and

$$\beta_{1m}^c = \sqrt{k_0^2 - \left(\frac{\pi}{a}\right)^2 - \left(\frac{m\pi}{W}\right)^2} = -j\alpha, \quad \eta_{1m}^c = \frac{\beta_{1m}^c \eta_0}{k_0}.$$

Forcing the appropriate boundary conditions renders the unknown coefficients.

C. Boundary Conditions

The boundary conditions between the waveguide and the crack apertures can be summarized by two cases. Case 1 is when the crack is fully within the waveguide aperture, and case 2 is when the crack is partially within the waveguide aperture as shown in Fig. 4(a) and (b), respectively.

1) Crack Fully Within the Aperture: When the crack is fully within the waveguide aperture as shown in Fig. 4(a), $(0 < c < b - W)$, the following boundary conditions must be satisfied for areas 1 and 2:

$$(E_y)^{\text{guide}} = 0 \begin{cases} 0 \leq x \leq a \\ 0 \leq y < c \text{ or } c' < y \leq b \\ z = 0 \end{cases} \quad (11)$$

and for area 3:

$$(E_y)^{\text{guide}} = (E_y)^{\text{crack}} \quad (12)$$

$$(H_x)^{\text{guide}} = (H_x)^{\text{crack}} \begin{cases} 0 \leq x \leq a \\ c \leq y \leq c' \\ z = 0 \end{cases} \quad (13)$$

and finally for area 4:

$$(E_y)^{\text{crack}} = 0 \begin{cases} 0 \leq x \leq a \\ c \leq y \leq c' \\ z = d \end{cases}. \quad (14)$$

2) Crack Partially Within the Aperture: When the crack is at the lower edge of the waveguide aperture as shown in Fig. 4(b), $(-W \leq c \leq 0)$, for areas 1, 3, and 4 similar boundary conditions as above must be satisfied and for area 2:

$$(E_y)^{\text{crack}} = 0 \begin{cases} 0 \leq x \leq a \\ c \leq y < 0 \\ z = d \end{cases} \quad (15)$$

When the crack is at the upper edge of the waveguide aperture $(b - W \leq c \leq b)$ the boundary conditions will be identical to those stated here.

D. Unknown Coefficients

Forcing the boundary conditions for case 1 (crack fully within the waveguide aperture) renders the following equations which, once simultaneously solved, the unknown coefficients and hence the field distribution at any point inside the waveguide can be determined as c varies between 0 and $(b - W)$:

$$A_{10} + 1 = \frac{W}{b}(1 - e^{-j2\beta_1 d})B_{10} \quad (16)$$

$$A_{10} - 1 + \sum_{m'=1}^{\infty} h(0, m')A_{1m'} = -B_{10}(1 + e^{-j2\beta_1 d}) \quad (17)$$

$$A_{1m} = -f(m)B_{10} + \sum_{m'=1}^{\infty} b(m, m')A_{1m'} \quad m = 1, 2, 3, \ldots \quad (18)$$

where

$$h(0, m') = \frac{\eta_1 b}{W\pi} \frac{1}{m'\eta_{1m'}^b} \left(\sin\frac{m'\pi c'}{b} - \sin\frac{m'\pi c}{b}\right) \quad (19)$$

$$p(m, n) = \frac{m(-1)^n}{b\pi\left(\frac{m^2}{b^2} - \frac{n^2}{W^2}\right)} \left(\sin\frac{m\pi c'}{b} + (-1)^{n+1}\sin\frac{m\pi c}{b}\right)$$
$$n = 1, 2, 3, \ldots \quad (20)$$

$$b(m, m') = \frac{-4}{bW\eta_{1m'}^b} \sum_{n=1}^{\infty} \frac{\eta_{1n}^c(1 - e^{-j2\beta_{1n}^c d})}{1 + e^{-j2\beta_{1n}^c d}} p(m, n)p(m', n) \quad (21)$$

$$f(m) = \frac{2}{m\pi}(e^{-j2\beta_1 d} - 1)\left(\sin\frac{m\pi c'}{b} - \sin\frac{m\pi c}{b}\right) \quad (22)$$

Similarly, by forcing the boundary conditions for case 2 the following equations are obtained. Once these equations are simultaneously solved the field expressions anywhere inside the waveguide can be obtained as c varies between $(-W)$ and 0 (or $b - W$ and b):

$$A_{1m} = B_{10}\frac{2}{m\pi}(1 - e^{-j2\beta_1 d})\sin\frac{m\pi c'}{b}$$
$$+ \sum_{n=1}^{\infty} \frac{2B_{1n}}{b}(1 - e^{-j2\beta_{1n}^c d})R(m, n) \quad (23)$$
$$m = 1, 2, 3, \ldots$$

$$B_{1n} = \frac{1}{1 - e^{-j2\beta_{1n}^c d}}\left[(1 + A_{10})\frac{2}{n\pi}\sin\frac{n\pi c}{W}\right.$$
$$\left.+ \frac{2}{W}\sum_{m=1}^{\infty} A_{1m}R(m, n)\right] \quad (24)$$
$$n = 1, 2, 3, \ldots$$

$$\frac{c'}{\eta_1}(A_{10} - 1) + \frac{b}{\pi}\sum_{m=1}^{\infty} \frac{A_{1m}}{m\eta_{1m}^b}\sin\frac{m\pi c'}{b}$$
$$= \frac{-c'B_{10}}{\eta_1}(1 + e^{-j2\beta_1 d})$$
$$- \frac{W}{\pi}\sum_{n=1}^{\infty} \frac{B_{1n}}{n\eta_{1n}^c}\left(1 + e^{-j2\beta_{1n}^c d}\right)\sin\frac{n\pi c}{W} \quad (25)$$

$$1 + A_{10} = \frac{c'}{b}\left(1 - e^{-j2\beta_1 d}\right)B_{10}$$
$$+ \frac{W}{b\pi}\sum_{n=1}^{\infty}\left(1 - e^{-j2\beta_{1n}^c d}\right)\frac{B_{1n}}{n}\sin\frac{n\pi c}{W} \quad (26)$$

where

$$R(m, n) = \frac{0.5}{\left(\frac{n}{W} + \frac{m}{b}\right)\pi}\left[(-1)^n\sin\frac{m\pi c'}{b} + \sin\frac{n\pi c}{W}\right]$$
$$+ \frac{0.5}{\left(\frac{m}{b} - \frac{n}{W}\right)\pi}\left[(-1)^n\sin\frac{m\pi c'}{b} - \sin\frac{n\pi c}{W}\right].$$

Having obtained the electric field distribution anywhere inside the waveguide, E_y can be calculated at $(x = a/2$ and $z = -\ell)$ which simulates the diode detector location. Thus, one can simulate the measurements by calculating $|E_y|^2$ assuming the
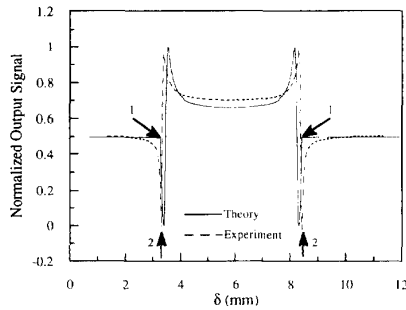
Fig. 5. Theoretical (————) and experimental (- - - - -) characteristic signals for a crack with $W = 0.84$ mm, $d = 1.53$ mm and $L = 10.7$ mm at 24 GHz.
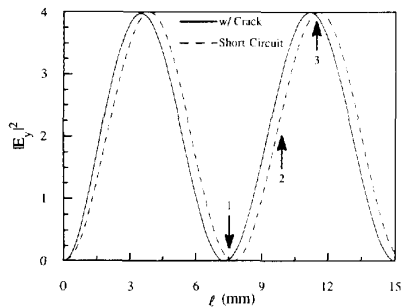

Fig. 7. Experimental characteristics signals for two cracks with $W = 0.277$ mm and different depths at 24 GHz.

Fig. 6. Calculated standing-wave pattern inside the waveguide at 24 GHz: (————) short circuit, (- - - - - -) crack with $W = 0.84$ and $d = 1.53$ at the center of the aperture.

diode detector is operating in its square-law region. Using the expressions for the incident and the reflected waves, one may also calculate the phase of the reflection coefficient at the aperture. Although the summations in (5), (6), (9) and (10) extend to infinity, in reality the number of required modes are finite and dependent on the crack dimensions and location within the waveguide aperture. This number increases when the crack size decreases and particularly when the crack is at the edge of the waveguide aperture. In the latter case more than a hundred modes may be required to satisfy the boundary conditions.

E. Comparison of the Theoretical and Experimental Results

To compare the results of the theoretical derivations with experimental results, $|Ey|^2$ for a crack with $W = 0.84$ mm and $d = 1.53$ mm was calculated at $\ell = 9.45$ cm away from the aperture (between a standing-wave null and maximum) at 24 GHz. Fig. 5 shows the normalized (with respect to the maximum value of each signal) results of the diode output voltage for the experimental case and $|E_y|^2$ for the theoretical case. The agreement between the two results is very good. The slight difference between the normalized signal levels is attributed primarily to the crack geometry not having 90° corners as assumed by the theory, and a small airgap present between the metal surface and the waveguide aperture during the measurements. The diode detector may not always operate in the square-law region (particularly for high input signal values) which may also attribute to this difference. The distance between the arrows marked 1 is equal
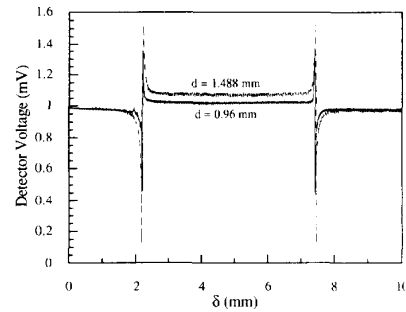
to the width of the crack plus the small dimension of the waveguide $(W + b)$. However, due to the causes mentioned above, experimentally the distance between the arrows marked 2 is approximated by $(W + b)$. Our experiments have shown that the error associated with measuring a thin crack width in this manner is less than 10% if the airgap is kept to a minimum. Therefore, the characteristic signal can be used to estimate crack width reasonably accurately.

Fig. 6 shows the calculated standing-wave pattern inside the waveguide, as a function of ℓ, for a short circuit and when the above crack is at the center of the aperture ($y = b/2$). The shift in the standing-wave pattern that was mentioned earlier is apparent. It is also evident that if the diode detector were at locations 1 and 3 there would be a minimal amount of signal (voltage) difference between the short-circuit and the crack-terminated cases. However, when the diode detector probes the standing wave at location 2 there will be a maximum signal (voltage) difference between the two cases.

Fig. 7 shows the characteristic signals for a long crack with $W = 0.277$ mm and two depths of 0.96 mm and 1.488 mm at 24 GHz. The results of these experiments indicate that the distance between the voltage reversals remains unchanged since this distance is primarily a function of the crack widths. However, the signal magnitudes in the middle of the aperture are different and once calibrated may serve as an estimator of crack depth.

Fig. 8(a) shows the calculated electric field distribution, $|E_y|(V/m)$, on a cracked metal surface with $W = 0.1$ mm and $d = 1$ mm at $y = b/2$ and three different locations on the x-axis at 90 GHz ($a = 2.54$ mm and $b = 1.27$ mm). As expected, the electric field at the center is maximum and diminishes towards the waveguide walls. Fig. 8(b) shows the same information at 10 GHz. It is evident that the same 100-micron wide crack is seen as a much wider perturbation on the metal plate at 90 GHz, as expected. Also note that the relative magnitude of the electric field is much smaller at 10 GHz than that at 90 GHz. At X-band the small crack is much further beyond cutoff. This type of theoretical simulation can be used to check, ahead of time, the feasibility of using a certain frequency range for detecting cracks with various width ranges.

As mentioned earlier, the ability to know the electric and magnetic field characteristics anywhere inside the waveguide not only renders information about the field magnitudes, but also about their phases. Fig. 9 shows the phase of the reflection
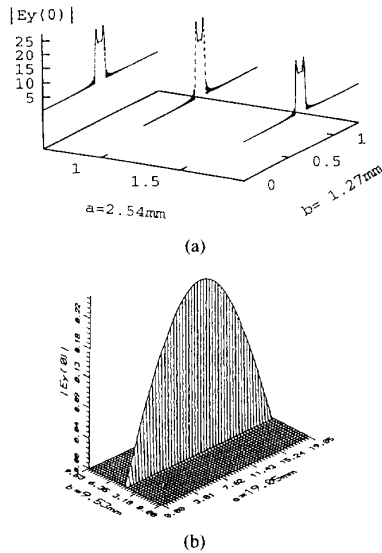
(a)

(b)

Fig. 8. Calculated electric field distribution (V/m) on a metal surface with a crack with $W = 0.1$ mm and $d = 1$ mm at (a) 90 GHz, (b) 10 GHz.
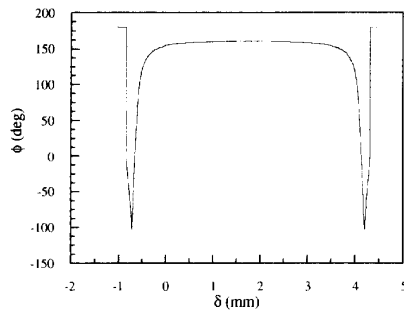

Fig. 9. Calculated phase of the reflection coefficient for a crack with $W = 0.84$ mm and $d = 1.53$ mm at 24 GHz.

coefficient (ϕ) for a crack with $W = 0.84$ mm and $d = 1.53$ mm. The change in the signal magnitude that was earlier referred to being due to a phase reversal is now evident. Thus, phase information can also be used for crack detection.

III. CONCLUSION

A new, simple and sensitive method for detecting long straight surface cracks in metals is described using an open-ended rectangular waveguide. This method which was es-tablished via numerous experimental investigations is also modeled electromagnetically. The modeling approach relies on properly forcing boundary conditions at the waveguide aperture. The significant phase reversal, when the crack is at the waveguide edges, makes this technique a very sensitive one for crack detection. Thus, this method is capable of detecting very thin cracks (fatigue and stress) at relatively low microwave frequencies. As expected, higher frequencies can be used to detect cracks with widths as narrow as a few microns. This technique is also suitable for estimating the

crack dimensions. This method may be used in environments such as aerospace, nuclear power plants, etc.

REFERENCES

[1] K. G. Boving, "NDE Handbook, Non-destructive examination methods for condition monitoring," *Teknisk Forlag A/S*, 1989.
[2] L. Feinstein and R. J. Hrby, "Surface crack detection by microwave methods," *6th Symp. Nondestructive Evaluation of Aerospace and Weapons Systems Components and Materials*, San Antonio, TX, 19 67.
[3] ——, *AIAA/ASME 9th Structure, Structural Dynamics and Materials Conference*, paper. #68-321, Apr. 1968.
[4] R. J. Hurby and L. Feinstein, "A novel nondestructive noncontacting method for measuring the depth of thin slits and cracks in metals," *Rev. Sci. Inst.*, vol. 41, pp. 679–683, May 1970.
[5] A. J. Bahr, "Microwave eddy-current techniques for quantitative non-destructive evaluation," in *Eddy-Current Characterization of Materials and Structures*, ASTM STP 722, pp. 311–331, 1981.
[6] ——, "Microwave eddy-current techniques for quantitative nondestruc-tive evaluation," in *Proc. DARPA/AF Rev. Progress in Quantitative NDE*, La Jolla, CA, July 1980.
[7] L. A. Robinson and U. H. Gysel, "Microwave coupled surface crack detector," Final Report, Contract DAAG-46-72-C-0019, SRI Project 1490, Stanford Research Institute, Menlo Park, CA, Aug. 1972.
[8] U. H. Gysel and L. Feinstein, "Design and fabrication of stripline microwave surface-crack detector in projectiles," Final Report, Contract DAAG-46-73-C-0257, SRI Project 2821, Stanford Research Institute, Menlo Park, CA, Aug. 1974.
[9] A. Husain and E. A. Ash, "Microwave scanning microscopy for non-destructive testing," in *Proc. 5th Eur. Microwave Conf.*, Hamburg, Germany, Sept. 1975, pp. 213–217.
[10] A. J. Bahr and J. P. Watjen, "Novel eddy-current probe development," Semi-Annual Report, Contract F33615-80-C-5025, SRI Project 1908, Menlo Park, CA, Feb. 1981.
[11] E. A. Ash and A. Husain, "Surface examination using a superresolution scanning microwave microscope," in *Proc. 3rd Eur. Microwave Conf.*, 1973, pp. c. 15.2.
[12] B. A. Auld, "Theory of ferromagnetic resonance probes for surface cracks in metals," G.L. Report 2839, E. L. Ginzton Laboratory, Stanford University, Stanford, CA, July 1978.
[13] ——, "Theoretical characterization and comparison of resonant-probe microwave eddy-current testing with conventional low-frequency eddy-current methods," in *Eddy-Current Characterization of Materials and Structures,*, ASTM STP 722, pp. 332–347, 1981.
[14] ——, "Ferromagnetic resonance flaw detection," *Pys. Tech.*, vol. 12, pp. 149–154, July 1981.
[15] D. M. Pozar, *Microwave Engineering*. Reading, MA: Addison-Wesley, 1990, ch. 4.

Chin-Yung Yeh received the B.S.E.E. degree from National Cheng-Kung University in 1970, the M.S.E.E. degree from the National Taiwan University in 1972, the Professional degree in electrical and computer engineering from the University of Michigan in 1982, and the Ph.D. degree in electrical engineering from Colorado State University.

He served on the board of directors of ROCSNT (ROC Society for Nondestructive Testing) from 1989 to 1991. Having been with the Institute of Nuclear Energy Research (INER) for more than 15 years, he is an NDT Level III in seven methods of INER and ROCSNT, and also an NDT Level III of ASNT. He has been involved in eddy current and ultrasonic testing research to improve the sizing technique for steam generator tubing and weld flaws. His current research interests is in the area of microwave NDT, particularly in metal surface/fatigue crack detection and sizing using microwave and millimeter wave techniques.
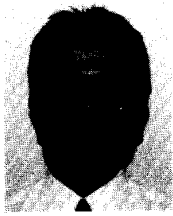
Reza Zoughi (S'85–M'86–S'86–M'87–SM'93) received the B.S.E.E., M.S.E.E., and Ph.D. degrees in electrical engineering (radar remote sensing, radar systems, and microwaves) from the University of Kansas in 1982, 1983, and 1987, respectively.

From 1981 until 1987 he was employed by the Radar Systems and Remote Sensing Laboratory at the University of Kansas in various capacities. He served as a graduate research assistant until 1983, and as an assistant project engineer until 1987. His experience at RSL included developing, building and operating various radar systems, data collection, and analysis. He has been involved in radar remote sensing research in the areas of determination of backscattering sources in various types of vegetation canopies (crops and trees) and surface targets and geology (lithology). Currently, he is an Associate Professor with the Electrical Engineering Department at Colorado State University, where he established the Applied Microwave Nondestructive Testing Laboratory. His current areas of research include nondestructive testing of material using microwaves, radar remote sensing of natural vegetation, and developing new electromagnetic probes to measure characteristic properties of material at microwave frequencies. He has published numerous articles in the field of microwave nondestructive testing.

Dr. Zoughi is a member of Sigma Xi; Eta Kappa Nu; and the American Society for Nondestructive Testing (ASNT), and a member of the editorial advisory committee for the International Advances in Nondestructive Testing (IANDT).